Seismic Testing of a Bridge Steel Truss Pier Designed for Controlled Rocking

Michael Pollino, M.ASCE[1]; and Michel Bruneau, F.ASCE[2]

Abstract: Shake table testing of a 1/5 scale model of a slender bridge steel truss pier that uses a controlled rocking approach as a means of seismic protection was conducted. The controlled rocking approach allows the pier to uplift from its base while passive energy dissipation devices (steel yielding devices or fluid viscous dampers) are implemented across the uplifting location to control the response. The fundamental static and dynamic bidirectional behavior of controlled rocking four-legged bridge piers has been developed and evaluated in past research. This paper discusses the experimental specimen's design, setup, and results of the testing. The testing program included the use of three sets of steel yielding devices and a set of fluid viscous dampers as the passive control devices. The specimens were subjected to ground motion records with increasing amplitude. The results of the testing were used to verify and further investigate the behavior of piers designed by the controlled rocking approach. Much of the fundamental behavior (self-centering, hysteretic behavior, and higher mode participation) are evident in the experimental results. Comparisons between the experimental results with design predictions and nonlinear time history analysis are made that show reasonable prediction of response.

DOI: 10.1061/(ASCE)ST.1943-541X.0000261

CE Database subject headings: Experimentation; Piers; Seismic effects; Energy dissipation; Trusses.

Author keywords: Experimental testing; Bridge piers; Seismic; Passive energy dissipation; Controlled rocking.

Introduction

The controlled rocking approach for seismic protection of bridge steel truss piers allows uplift and rocking of piers on their foundation while displacement-based steel yielding devices or fluid viscous dampers are used at the uplifting location to control pier response to within allowable limits. The devices can be calibrated to capacity protect the existing vulnerable members of the pier and the foundation of the structure. The system provides a significant restoring force that can allow re-centering of the structure with proper selection of device properties. Prior research has developed the fundamental behavior and simplified methods for design of controlled rocking two-legged (Pollino and Bruneau 2007) and four-legged (Pollino and Bruneau 2010) bridge steel truss piers. This prior research was used for the design of an experimental specimen and setup of the testing program to further verify the approach as a seismic protection strategy.

The scaled model used for testing is based on a generic prototype bridge steel truss pier for a typical two-lane highway bridge. Following similitude scaling requirements and based on the available laboratory resources, a 1/5-length scale model was used for testing. The resulting specimen was 6.09 m in height and had a height-to-width aspect ratio of 4. Seismic testing was conducted on a six-degree-of-freedom (6DOF) shaking table in the Structural Engineering and Earthquake Simulation Laboratory (SEESL) located at the University at Buffalo. Steel yielding devices and fluid viscous dampers were used as the passive energy dissipation devices during the testing. The model was subjected to both historical ground motion records and a synthetically generated motion. The results of the experimental testing program are discussed followed by a comparison of experimental results with design and analytical response predictions.

Prototype Pier

Prototype pier properties are based on a brief review of drawings of existing bridges supported on steel truss piers. The prototype bridge pier is assumed to support a segment of a two-lane highway bridge deck between the bridge's abutments. The pier is assumed to have a tributary inertial mass in the longitudinal and transverse directions equal to its vertical mass. In general, steel truss pier diagonals tend to have a constant cross section in each pier panel and pier legs are continuous over its height. Connection of the bridge deck to pier varies considerably depending on the type of bridge bearing used. For the purpose of this study, the connection of the bridge deck to pier is assumed to be pin-connected near the top of each pier leg. Prototype pier properties deemed relevant for dynamic testing are given in Table 1. Photographs of two-legged and four-legged bridge piers of this type are shown in Fig. 1. Incidentally, these piers have been retrofitted by allowing them to rock (Dowdell and Hamersley 2001), although the specimens are not meant to be exact model replicas of those specific piers.

[1]Assistant Professor, Dept. of Civil Engineering, Case Western Reserve Univ., Cleveland, OH 44106; formerly, Simpson, Gumpertz, and Heger Inc., 41 Seyon St., Bldg. 1, Suite 500, Waltham, MA 02453 (corresponding author). E-mail: mcp70@case.edu

[2]Professor, Dept. of Civil, Structural, and Environmental Engineering, Univ. at Buffalo, Buffalo, NY 14260. E-mail: bruneau@buffalo.edu

Note. This manuscript was submitted on March 24, 2009; approved on June 10, 2010; published online on June 15, 2010. Discussion period open until May 1, 2011; separate discussions must be submitted for individual papers. This paper is part of the ***Journal of Structural Engineering***, Vol. 136, No. 12, December 1, 2010. ©ASCE, ISSN 0733-9445/2010/12-1523–1532/$25.00.

Table 1. Prototype and Model Pier Properties

Quantity	Prototype	Model	
		Required[a]	Provided[b]
Height, h	29.3 m	5.86 m	6.09 m
Width, d	7.32 m	1.46 m	1.52 m
Aspect ratio, h/d	4.0	4.0	4.0
Inertial mass, m_x (and m_y)	1,730 kN/g	69.2 kN/g	80.1 kN/g
Gravitational weight, w_{mz}	1,730 kN	69.2 kN	80.1 kN
Material modulus, E	200 GPa	200 GPa	200 GPa
Lateral stiffness, k_{ox} (and k_{oy})	12.6 kN/mm	2.52 kN/mm	3.00 kN/mm
"Fixed-base" lateral period, T_{ox} (and T_{oy})	0.74 s	0.33 s	0.33 s
"Fixed-base" vertical period	0.13 s	0.058 s	0.040 s
Vertical "shearing" period, T_v	0.12 s	0.054 s	0.062 s

[a]Required model properties for similitude requirements.

[b]Theoretical model properties provided by the specimen.

Experimental Model Scale

The artificial mass simulation scaling law, used in many experimental tests investigating response of structures to earthquakes (Harris and Sabnis 1999), has also been followed here. For constant acceleration scaling and since the model is made of the same material as the prototype (steel), the acceleration scale factor, λ_a, and the elastic modulus scale factor, λ_E, are equal to one. Using this scaling law, the required model properties and properties provided after modifications required for controlled rocking design are shown in Table 1. To implement energy dissipation devices of credible dimensions for controlled rocking, it was desirable to test the largest model possible, its height being ultimately controlled by the vertical distance from the shake table to a workable crane clearance height ($\sim$7 m). For this purpose, an existing slender steel specimen in the laboratory, which had been used in past testing, was found to be available and provided most of the required relevant model properties reasonably well. The resulting model (approximately 6 m tall) provided a length scale factor of 5 based on the prototype height of 29.3 m.

The primary similitude requirements targeted were the "fixed-base" lateral and vertical periods of the model (T_{om} and T_{Lm}), the vertical shearing mode period (T_{vm}), and the applied and restoring forces of the model. Although an added mass of 69.2 kN/g was required by similitude, steel plates totaling 80.1 kN/g were used since they were readily available in the laboratory. A photograph of the specimen on the 6DOF shake table is shown in Fig. 2.

Specimen Design and Boundary Conditions

The existing specimen structure (originally designed for different purposes) was modified to satisfy similitude and strength requirements, to allow rocking at the base, and to provide adequate boundary conditions. Modifications, required primarily at the base of the specimen, included replacing the column base plates, and adding column flange cover plates, column web doubler plates,

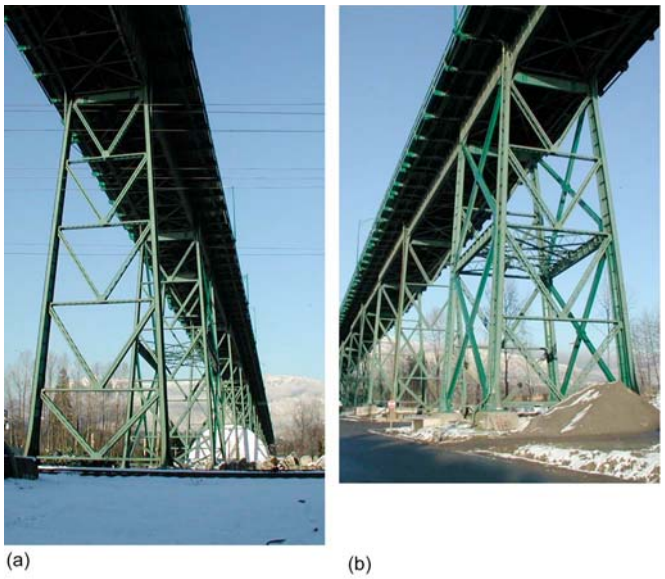

Fig. 1. Typical prototype steel truss bridge piers (Courtesy of Bruce Hamersley, Klohn Crippen Berger Engineering): (a) two-legged piers; (b) four-legged pier

Fig. 2. Rocking steel truss pier specimen on shake table

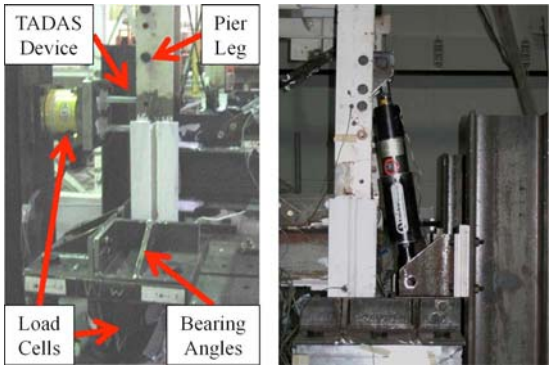

Fig. 3. Base connection

beam-column transverse stiffeners, and a base perimeter beam (collector beam). Specimen details and boundary conditions were designed as described below.

Base Connection

The connection at the base of the pier legs was detailed to resist translation (sliding) in the two horizontal directions, to allow vertical translation (uplift) from the support during rocking, and to accommodate load cells placed beneath the base of each pier leg to record pier base reactions during testing. Connection of the pier base to the load cells was done through a horizontal bearing "pit" connection using angle members bolted to the top of each load cell as shown in Fig. 3. No resistance was provided vertically through this connection except for a negligible amount of friction that could have occurred along an angle's leg as the pier leg uplifts. The angles were only placed on the two outer sides of the load cells in contact with the two outer sides of the column base plates such that the horizontal shear force of the pier would not be transferred at the base of the uplifting pier legs. Such placement of the angle members limited the amount of contact the base of the pier legs had with the base connection during uplifting while resisting horizontal shear at the base of the other legs and thus preventing sliding. The base connection was also capable of transferring torsion in the pier that may develop as a result of minor misalignment of the mass plates and center of pier stiffness or errors in control of the shake table however no significant torsional response was observed during testing.

Pier Diagonals

Pier diagonals were designed to meet similitude and strength requirements. The existing specimen had moment-resisting beam-column connections such that when the pier diagonals were added, the specimen acted as a braced moment frame. The cross-sectional area of the diagonal members (A_{dmi}) were sized such that the fixed-base and vertical periods of the specimen were close to that required by similitude and would have the required tension strength to resist demands during the rocking response. Considering an *X*-braced configuration, resulted in the use of high-strength circular threaded rod (ASTM A193 B7, σ_y =869 MPa) diagonal bracing members with a 9.5-mm diameter. Buckling strength did not scale proportionally, and these members, with effectively no buckling strength, would have undergone elastic buckling during testing, creating a tension-only bracing system. To remediate this problem, all diagonal bracing members were pretensioned to a prescribed axial force level such that these members would remain in tension throughout testing. The pretensioning was achieved by using right and left-handed threaded rod for the bracing members and connecting them with a reverse threaded hex coupler. (Note that it is not implied here that diagonal members be pretensioned for design or retrofit of actual structures—only that they be designed to remain elastic by providing a compressive buckling strength exceeding the calculated axial forces in the members.) A strain gauge was attached on one face of the hex coupler to measure strain and determine pretensioning force during installation and to measure member force during testing.

Mass Connection

Connection of a bridge deck to its piers is typically achieved through the use of some form of bearing (rocker, pot, elastomeric, cylindrical, spherical, AASHTO 1998). Each type of bearing transfers gravity loads and seismic inertia forces between the deck and pier by different mechanisms. For the specimen, the steel mass plates were connected to the pier using 16–9.5 mm diameter, fully tensioned high-strength threaded rods (ASTM A193 B7) through the 2–90 mm thick steel mass plates, a double concave hardened steel bearing, mild-steel connection plate, and 2–19.1 mm plate washers. The shear force was transferred through friction between each piece.

Passive Energy Dissipation Devices

Passive energy dissipation devices were installed between the pier foundation (i.e., the shake table in this case) and the base of each pier leg. Two types of devices were used in this experimental study, namely: steel yielding devices and viscous dampers.

Steel Yielding Devices

Various steel yielding devices were sized to provide a range of local strength ratios (η_L) and observe the influence on response. The local strength ratio is an important parameter in design of the controlled rocking pier using steel yielding devices and is defined for four-legged piers as

$$\eta_L = \frac{F_d}{w_v/4} \tag{1}$$

where F_d=plastic capacity of the device and w_v=vertical weight tributary to the pier. Steel yielding devices with bilinear hysteretic behavior were designed with connections to apply only a vertical force to the base of the pier legs. Key design parameters for the devices are the plastic device force, elastic stiffness, and maximum allowable vertical displacement. Different types of steel yielding devices were considered for these experiments, including buckling-restrained braces (AISC 2005) and shear panel devices (Zahrai and Bruneau 1998). However, such braces and shear panels could not be easily/reliably manufactured/fabricated at this scale.

The number of design parameters that define the behavior of TADAS devices (Tsai et al. 1993) provide more dimensioning freedom and allowed a device that could be fabricated at this scale. TADAS devices consist of cantilever triangular plates bent about their minor axis that yield in flexure uniformly along their length when a shear force is applied at their free end. The plastic shear force of the device, $V_{pT}(=F_d)$, can be shown to equal

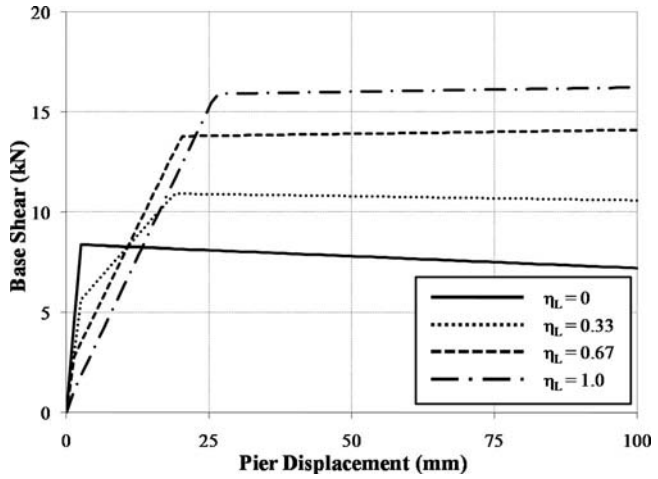

Fig. 4. Unidirectional static pushover curves for experimental specimen with steel yielding devices

$$V_{pT} = \frac{N_T t_T^2 b_T F_{yT}}{4L_T} \tag{2}$$

where N_T=number of plates; t_T=plate thickness; b_T=plate width at fixed support of device; F_{yT}=yield stress of steel (50 ksi, ASTM A572 Gr. 50); and L_T=length of plates from fixed support to point of loading. The elastic stiffness is equal to

$$k_{eT} = \frac{E \cdot b_T \cdot N_T}{6}\left(\frac{t_T}{L_T}\right)^3 \tag{3}$$

Results of component and sub-assemblage testing (Tsai et al. 1993) has shown TADAS devices able to withstand rotations of 0.30 rad, where the device rotation, γ_T, is defined as

$$\gamma_T = \Delta_{upL}/L_T \tag{4}$$

Three sets of devices were designed and fabricated with local strength ratios ($\eta_L = V_{pT}/w_v/4$) of 1.0, 0.67, and 0.33. For comparison, the static hysteretic pushover curve of the experimental specimen for a free-rocking specimen (η_L=0) and with each set of steel yielding devices attached, considering 2nd cycle response (Pollino and Bruneau 2007) and P-Δ effects is shown in Fig. 4. Table 2 lists the key dimensions and design parameters for each set of devices.

Fluid Viscous Dampers

The controlled rocking response with fluid viscous dampers was also investigated using a single set of nonlinear viscous dampers. The viscous dampers were implemented in a very similar manner to the TADAS devices, as seen in Fig. 3. The key design parameters using such devices are the peak output force and maximum stroke of the damper. Nonlinear dampers of this type have a force output, dependent on the velocity across the damper equal to

$$F_{vd} = c \cdot \text{sgn}(v_d) \cdot |v_d|^{\alpha_d} \tag{5}$$

where c=damping coefficient of 1.32 kN(s/mm)$^{\alpha}$; v_d=relative velocity across the two ends of the damper; sgn=sign function; and α_d=damping exponent of 0.50. The selected dampers had a stroke of ±31.75 mm, although when implemented in the controlled rocking system considered here, they only extended in a single direction as the pier legs uplifted from their base.

Loading System, Instrumentation, and Data Acquisition

The shake table used for this project can achieve a nominal acceleration performance of 1.15 g in each of its horizontal and vertical directions with a 20-t rigid specimen, with maximum displacements of ±5.9 and ±2.9 in. in the horizontal and vertical directions, respectively.

Instrumentation used included accelerometers, string potentiometers, eight strain gauge based load cells, and strain gauges. The entire specimen was supported on four large-capacity load cells that measured the base reactions (seen in Fig. 3). During testing with the viscous dampers, additional load cells were attached in-line with the damper shaft to measure damper force. A Krypton K600 high performance dynamic mobile coordinate measurement machine was used to measure displacements near the base of the structure. All instrumentation signals were low-pass filtered at a cut-off frequency of 50 Hz and sampled at a rate of 128 Hz.

Base Excitation

The input excitation to the shake table included banded white noise excitation for dynamic characterization of the specimen, and seismic ground motion histories for evaluation of response. The seismic ground motions included the Newhall record from the 1994 Northridge earthquake and a synthetically generated

Table 2. TADAS and Viscous Damper Properties Used in the Experiments

TADAS								
η_L	N_T	L_T (mm)	t_T (mm)	b_T (mm)	k_T (kN/mm)	Δ_{pT} (mm)	γ_{design}	$\mu_{L,design}$
1.0	4	88.9	9.53	50.8	8.34	2.13	0.15	6.3
0.67	2	88.9	11.1	54.0	7.02	1.83	0.30	14.6
0.33	1	88.9	11.1	54.0	3.52	1.83	0.30	14.6

Viscous dampers			
c [kN(s/mm)$^{\alpha}$]	α	$\Delta_{d,max}$ (mm)	$F_{d,max}$ (kN)
1.32	0.50	63.5	44.5

record (tests performed with other seismic motions and other forms of base input (see Pollino and Bruneau 2008 for details) are not discussed here due to space constraints). All three acceleration components (two horizontal and vertical) from each record were simultaneously applied to each specimen. Per similitude scaling laws, acceleration amplitude was unscaled and the time of the record was scaled by a factor of 2.24. The target pseudoacceleration response spectrum of each component of motion for each record, at model scale, is shown in Fig. 5. Due to differences in the target input acceleration history and that actually achieved by the shake table during testing, the recorded table accelerations and resulting spectra are used for comparison with analytical and design predictions.

Testing Program

The test setups considered included three sets of steel yielding devices (η_L=0.33, 0.67, and 1.0), a set of nonlinear viscous dampers, and tests on the free-rocking pier (η_L=0). Each setup was first subjected to a white noise test followed by an earthquake record amplitude scaled to 35% of the target value simply to verify instrumentation functionality, table performance, and specimen behavior. Then, the Newhall record was run at 100% amplitude, followed by the Synthetic record also at 100%. After that, different excitation records were run at higher amplitude (150% or more) for different setups. All tests were followed by a white noise test to observe any changes in the dynamic properties of the specimen.

Experimental Results

Test results presented below include identification of the specimen's dynamic characteristics from white noise excitations, and results from seismic excitation. The peak response of each test is compared with design predictions and advanced analysis methods.

Identification of Dynamic Characteristics

Response of the model structure during white noise excitation was limited to the elastic range of response, thus providing the fixed base pier properties; it could not capture system behavior after uplift. The mode shapes, frequencies, and damping ratios of the structure were determined using a modal identification technique based on pier transfer function response. The transfer functions are defined as the ratio of the cross and power spectra between the top of pier and table accelerations in a particular direction, also known as the H_1 estimator (Bendat and Piersol 1980).

Initial white noise tests showed that the specimen had a fixed-base frequency of approximately 2.5 Hz (T_{om}=0.40 s). Fig. 6 shows changes in the specimen's frequency through the testing program. The vertical axis of the figure is the frequency calculated from the white noise test (f_i) normalized by the frequency calculated from the first test (f_1=2.5 Hz) in that particular orientation (X, Y, or Z). As seen in the figure, the frequency changes by less than 5% from the initial test in each setup, indicating no damage to the model specimen, except for white noise test 5 which exhibits a significant drop in frequency relative to the initial test. White noise Test 5 was performed following the seismic tests of the setup with η_L=1.0. Since the strength of the devices in this setup is nearly equal to or greater than the structures tributary weight, the structure was likely partially supported up on the devices following the tests with η_L=1.0 and the specimen's response would be controlled by its 2nd cycle properties (Pollino and Bruneau 2007). After these devices were removed and the devices with η_L=0.33 were attached for the next setup, the following white noise test showed that the system returned to 93% of its initial frequency.

The specimen's inherent equivalent viscous damping, calculated both by the frequency response analysis using the half-

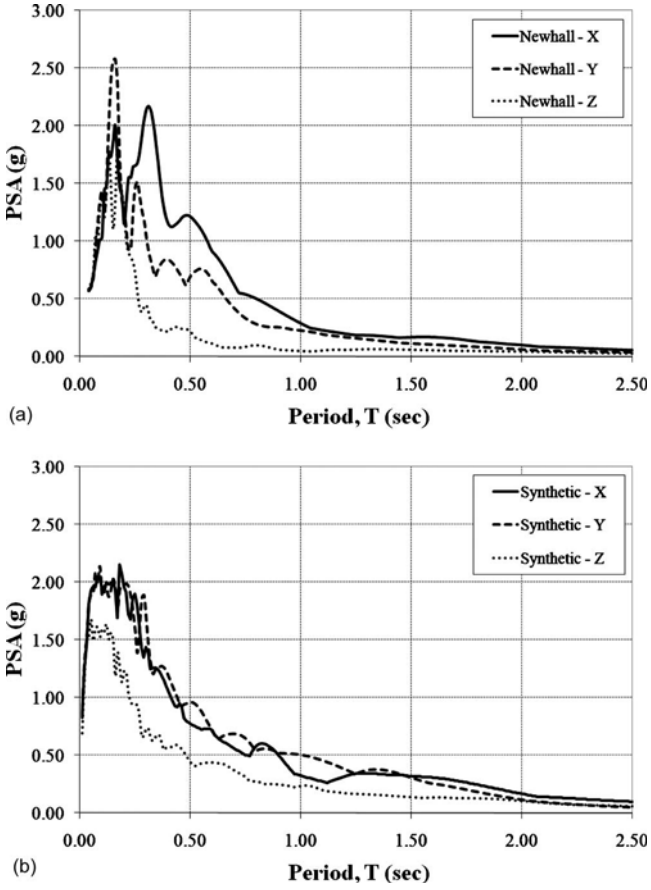

Fig. 5. Target pseudoacceleration spectra in model scale: (a) Newhall record; (b) synthetic motion

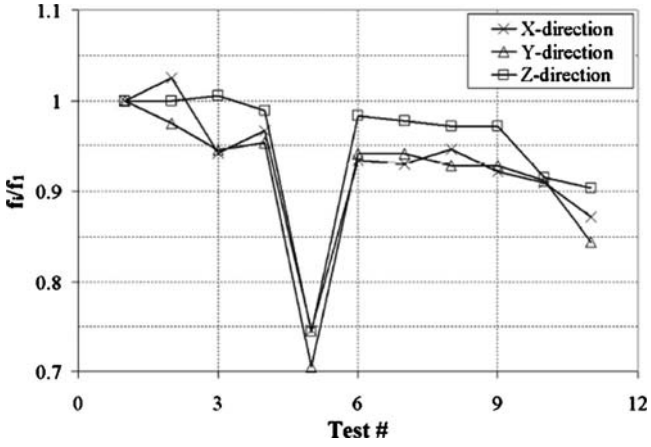

Fig. 6. Specimen fixed-base frequency throughout testing program

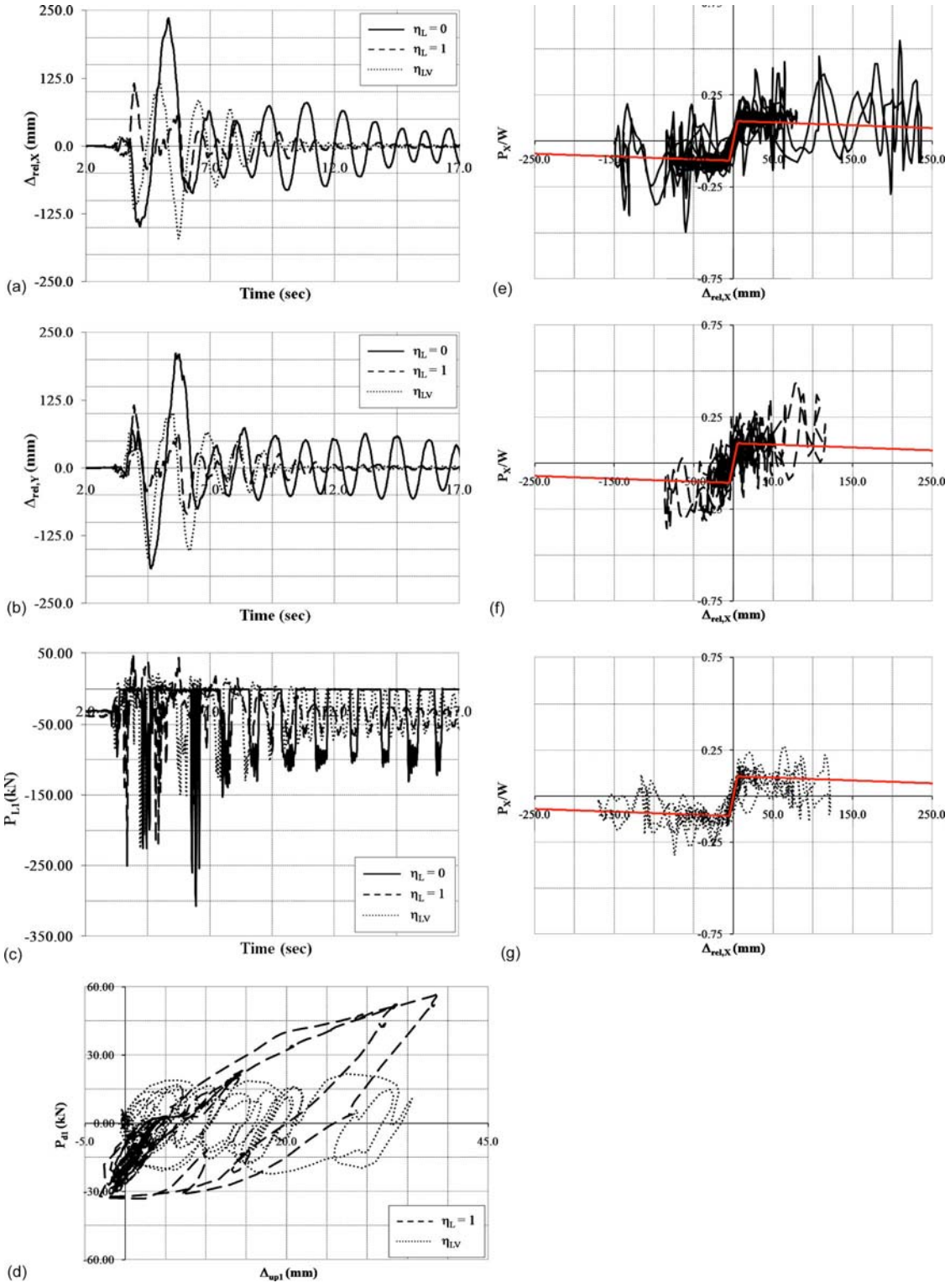

Fig. 7. Experimental response comparison, for synthetic motion scaled to 150%: (a) relative pier *X*-displacement; (b) relative pier *Y*-displacement; (c) pier leg axial force; (d) device hysteretic behavior; (e) global hysteretic behavior, $\eta_L=0$; (f) global hysteretic behavior, $\eta_L=1.0$; and (g) global hysteretic behavior, η_{Lv}

power (bandwidth) method and by the logarithmic decrement method (Clough and Penzien 1975), was determined to be approximately 2.5% of critical.

Example Response History Results

An example set of response history results is shown in Fig. 7 for the Synthetic record input scaled to 150% of the target motion. Response of the pier with no control devices attached ($\eta_L=0$, free-rocking), steel yielding devices with $\eta_L=1.0$ attached, and viscous dampers attached (η_{Lv}) at the base are shown in the figure. The figure shows the pier relative displacement in the two horizontal directions, pier leg axial force (for a single leg), device hysteretic behavior (for a single device), and the global pier hys-

teretic behavior. Also, overlain on the global pier hysteretic behavior is the static pier pushover curve. The relative pier displacement is shown to return to zero following the input excitation due to the self-centering ability of the system (final response of the free rocking test damps out much more slowly but eventually returned to zero with no residual displacement). The higher mode dynamic effects that are discussed in Pollino and Bruneau (2008) are evident in global hysteric pier behavior and the pier leg axial forces.

Comparison of Experimental Results with Nonlinear Time History Analysis

The response of the experimental specimen was predicted analytically using nonlinear time history analysis. Comparison is made between the peak experimental response quantities and peak response results from time history analysis.

The approach for analytical modeling is described in detail in Pollino and Bruneau (2010) however modeling directly relevant to the experimental model is discussed here. The model mass is lumped in a single node at the geometric centroid of the steel mass plates and includes their mass moments of inertia (thus the effects of torsion are accounted for). The diagonal braces are modeled by members that can only resist axial forces (in tension and compression). The pretensioning force in the members is applied in the model using a temperature loading on the members to match the prescribed axial force applied on the specimen by pretensioning (using reverse threaded couplers). Since the diagonal members could resist both tension and compression forces (without buckling) in the analytical model, the temperature loading was applied only to achieve the correct internal forces in the specimen (not required otherwise analytically to prevent buckling). The analytical model was excited dynamically by applying acceleration histories to the fixed supports. In light of the aforementioned discrepancies observed between the target and achieved motions during testing on the shaking tables, the acceleration of the table recorded during each test (X, Y, and Z) was supplied to the analytical model as the base input (as opposed to the target motion).

The experimental and time history analytical results are compared in terms of peak relative displacement (X- and Y-directions), peak uplift displacement, peak pier leg axial force, and peak base shear force (X- and Y-directions) in Fig. 8 where subscripts "Exp" refers to the experimental results and "TH" refers to the results from time history analysis. Separate data points are shown on the figures for each seismic test. A solid, dark line is plotted for $Q_{\text{Exp}}=Q_{\text{Analytical}}$ (Q referring in general to a peak response quantity). This line defines a boundary for each data point that represents conservative (below line) and unconservative (above line) prediction of response. The second solid line represents the average difference of the data from this boundary and is defined in general as

$$Q_{\text{Exp}} = Q_{\text{Analytical}} + \mu_{\Delta Q} \tag{6}$$

where $\mu_{\Delta Q}$=mean difference between experimental and analytical data points and is defined as

$$\mu_{\Delta Q} = \frac{\sum_{i=1}^{n} [Q_{\text{Exp}}(i) - Q_{\text{Analytical}}(i)]}{n} \tag{7}$$

where n=total number of tests run for the cases considered. Two dotted lines are also shown on the plots, corresponding to the mean difference plus and minus one standard ($\sigma_{\Delta Q}$) such that

$$Q_{\text{Exp}} = Q_{\text{Analytical}} + \mu_{\Delta Q} \pm \sigma_{\Delta Q} \tag{8}$$

where $\sigma_{\Delta Q}$ is defined as

$$\sigma_{\Delta Q} = \sqrt{\frac{\sum_{i=1}^{n} [Q_{\text{Exp}}(i) - Q_{\text{Analytical}}(i) - \mu_{\Delta Q}]^2}{n-1}} \tag{9}$$

Figs. 8(a–c) show a good correlation between the experimental and time history analysis results in terms of maximum relative and uplifting displacement. More scatter in the data exists for the maximum force demands [Figs. 8(d–f)] with some points that deviate significantly.

Note that better correlation exists for base shear results for cases with viscous dampers attached vertically at the base (circle data points in Figs. 8(e and f) than for the case of free rocking (square data points) or η_L=0.33 (diamond data points).

Comparison of Experimental Results with Design Predictions

The simplified method of analysis and design equations derived from fundamental research and presented in Pollino and Bruneau (2010) are used to predict the dynamic response of the experimental specimen and are compared with test results. The pier displacement is predicted using this simplified method of analysis ($\Delta_{\text{rel,Design}}$) and is based on the capacity spectrum analysis method. Use of this type of analysis method is more useful for design purposes as it doesn't require time history analysis. Other relevant response quantities ($P_{u,\text{Design}}, P_{uL,\text{Design}}, \Delta_{up,\text{Design}}$) are also predicted using design equations presented in Pollino and Bruneau (2010).

Comparison of the experimental and the simplified methods of analysis are made in an identical manner as was done for the time history results. The response quantity predicted by the simplified analysis and design equations (design quantity) is plotted on the horizontal axis while the experimental response quantity is the vertical coordinate. Comparison of peak response between the experimental results and design equations are shown in Fig. 9.

Force Response

The maximum force response shown in Figs. 9(d–f) is predicted reasonably accurately and conservatively in most cases by the simplified methods of analysis. The pier leg axial force and base shear results show that the design equations predict an increase in force response for increasing strength ratio (η_L), however, smaller increases were observed in the experimental results for larger strength ratios. For instance, the pier leg axial force results [Fig. 9(d)] show this trend (even though the predictions are nearly all conservative).

Some of the conservatism observed can be explained. For example, following the derivation of the design equations [Eqs. (19) and (20)] from (Pollino and Bruneau 2010) that predicts the maximum developed base shear and pier leg axial force, the dynamic effects due to impact, uplift, and vertical excitation are combined with a modal combination rule and added to the forces developed

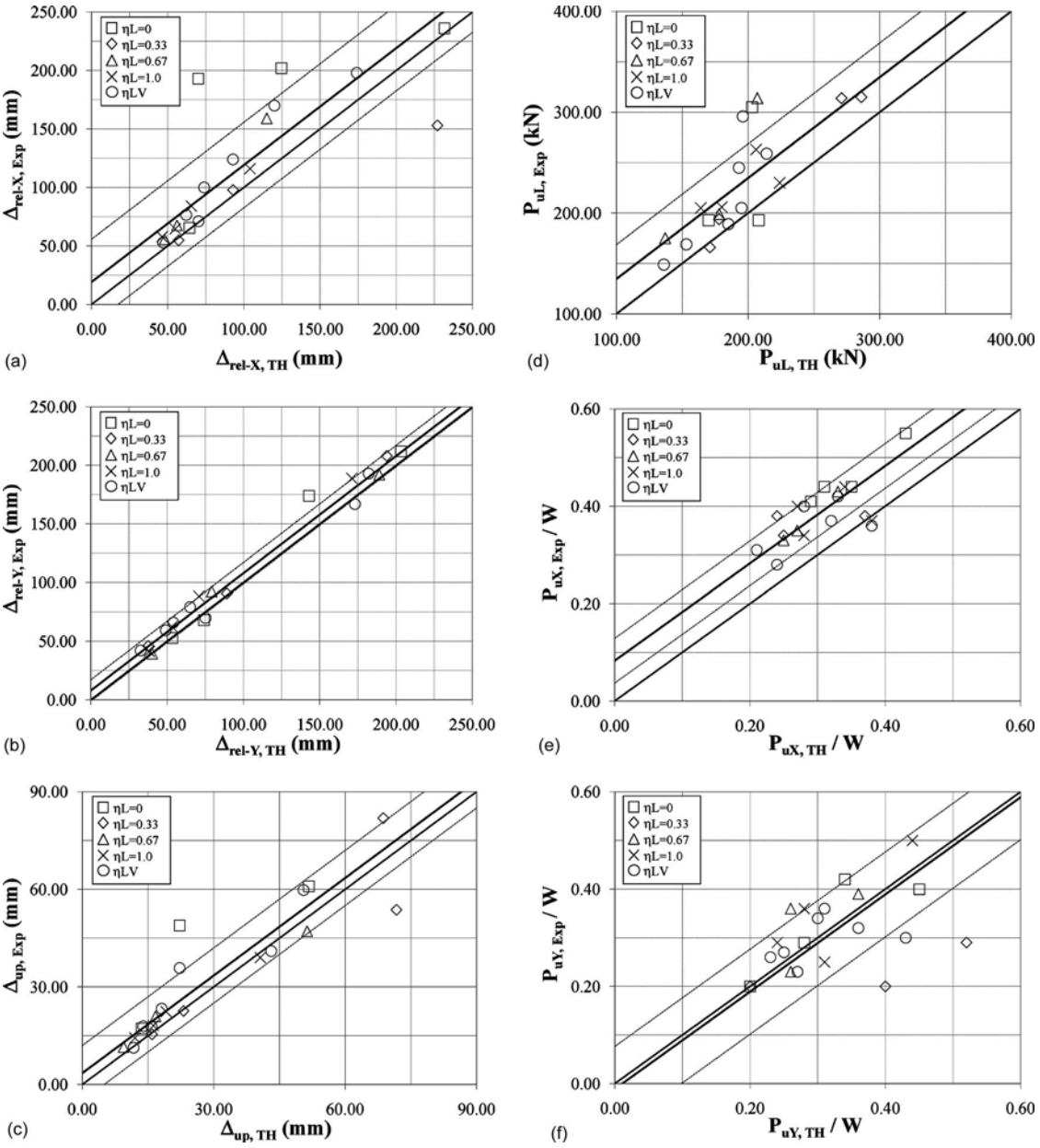

Fig. 8. Experimental results comparison with time history analysis: (a) pier relative displacement in *X*-direction; (b) pier relative displacement in *Y*-direction; (c) pier leg uplifting displacement; (d) pier leg axial force; (e) pier base shear force in *X*-direction; and (f) pier base shear force in *Y*-direction

assuming the bidirectional plastic yield mechanism has formed (uplift and yielding of all steel yielding devices). The energy dissipating devices were designed such that the design level motion would lead to development of the plastic mechanism, and the maximum uplifting displacements were limited by deformations to the devices. However not all tests reached the design level thus the displacement response may not have been large enough to develop the plastic mechanism. It is also conservative to assume that the combination of the dynamic effects is occurring when the structure is in the state at which the yield mechanism has formed. This is especially true for the cases with a higher strength ratio (η_L), for which the structure spends less time in a position in which the yield mechanism has developed. In the case of bidirectional response, the structure spends even less time in the plastic mechanism state.

Displacement Response

Displacement results in Figs. 9(a–c) show that the simplified analysis method yields displacement results that compare closely to the experimental results until the predicted relative pier displacements exceeded approximately 100 mm where the experimental results were larger than predicted by 150 to 200%. With exception of two data points, all of these outlier points for the

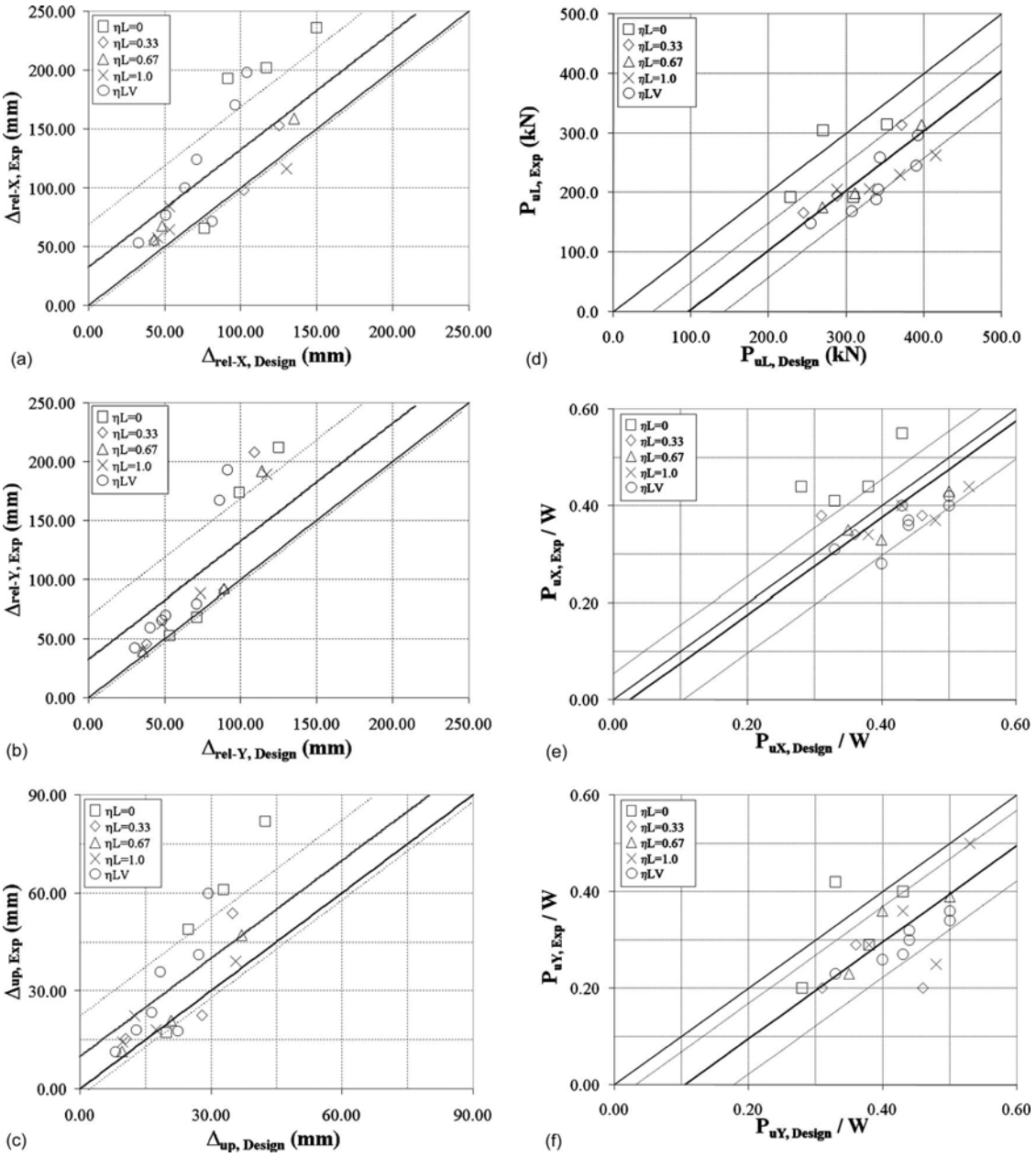

Fig. 9. Experimental results comparison with design predictions: (a) pier relative displacement in *X*-direction; (b) pier relative displacement in *Y*-direction; (c) pier leg uplifting displacement; (d) pier leg axial force; (e) pier base shear force in *X*-direction; and (f) pier base shear force in *Y*-direction

relative displacement are for $\eta_L=0$ or the viscous damper tests. Taking a closer look at the use of the capacity spectrum method for these cases, it was found that for those systems, having large secant periods, low yield strength, and very low or negative post-tyield stiffness (due to P-Δ effect), the intersection of the spectral capacity and demand curves occurs in a range of the spectrum that does not match the target spectrum well. While the predicted response depends on the intersection of these two curves, the behavior of the system is not completely dependent on this range of the response spectrum and will also depend on the frequency content of the motion prior to uplift and yield which is not considered in this simplified analysis method.

Conclusions

An experimental program was performed for a 1/5-length scale, four-legged bridge pier specimen. The passive control devices used included steel yielding devices (TADAS) and fluid viscous dampers. The specimen was subjected to three components of seismic ground motion ($X+Y+Z$) using both recorded and synthetically generated motions. White noise testing revealed that the fixed-base horizontal period of the pier was equal to 0.40 s and that the pier had an inherent damping of approximately 2.5% of critical. Many seismic tests were performed that generated a maximum relative pier displacement of 236 mm (3.9% drift) and 82 mm of uplift. The specimen was not damaged during the testing program and recentered following each test.

The results of the testing program were used to assess the adequacy of the design predictions and analytical modeling discussed in Pollino and Bruneau (2010) and to observe overall dynamic behavior. There were a few instances in the prediction of the maximum displacement of the experimental specimen in which the simplified analysis approach provided displacements 30–50% below that observed in experiments. Also, the maximum uplifting displacements may be influenced by the vertical ground displacements which are not accounted for in the prediction of displacements and which primarily affect deformations of the devices.

Design equations for combination of multicomponent, multimodal force effects were found to provide conservative, yet reasonably accurate, prediction of response. The design equations assume development of the controlled rocking pier's yield mechanism. Some results of experimental tests for systems that underwent bidirectional response showed significant deviation in force response from that predicted by the design equations however this was mostly for cases in which the pier was not subjected to the design level of excitation. In general, the response of systems that achieved a global displacement ductility (μ_{G2}) greater than approximately three matched reasonably accurately with the predicted force response.

The development of the bidirectional yield mechanism and support of the pier on a single leg along with the effects of vertical excitation can cause significant axial forces in the pier legs such that they may likely require strengthening. However, a conventional seismically designed pier undergoing bidirectional yielding may subject the leg to similar levels of axial force and would also require design of a significant uplift force at the anchorage connection.

Acknowledgments

This paper was supported in part by the Federal Highway Administration under Contract No. DTFH61-98-C-00094 to the Multidisciplinary Center for Earthquake Engineering Research. However, any opinions, findings, conclusions, and recommendations presented in this paper are those of the writers and do not necessarily reflect the views of the sponsors.

References

AASHTO. (1998). *LRFD bridge design specifications*, Washington, D.C.

AISC. (2005). *Seismic provisions for structural steel buildings*, Chicago.

Bendat, J. S., and Piersol, A. G. (1980). *Engineering applications of correlation and spectral analysis*, Wiley, New York.

Clough, R. W., and Penzien, J. (1975). *Dynamics of structures*, McGraw-Hill, New York.

Dowdell, D., and Hamersley, B. (2001) "Lions' gate bridge north approach: Seismic retrofit: Behaviour steel structures in seismic areas." *Proc., 3rd Int. Conf. STESSA 2000*, Balkema, Rotterdam, The Netherlands, 319–326.

Harris, H., and Sabnis, G. (1999). *Structural modeling and experimental techniques*, 2nd Ed., CRC, Boca Raton, Fla.

Pollino, M., and Bruneau, M. (2007). "Seismic retrofit of bridge steel truss piers using a controlled rocking approach." *J. Bridge Eng.*, 12(5), 600–610.

Pollino, M., and Bruneau, M. (2008). "Analytical and experimental investigation of a controlled rocking approach for seismic protection of bridge steel truss piers." *Technical Rep. No. MCEER-08-0003*, Multidisciplinary Center for Earthquake Engineering Research, State Univ. of New York at Buffalo, Buffalo, N.Y.

Pollino, M., and Bruneau, M. (2010). "Bidirectional seismic behavior of controlled rocking four-legged bridge steel truss piers." *J. Struct. Eng.*, 136(12), 1512–1522.

Tsai, K. C., Chen, H. W., Hong, C. P., and Su, Y. F. (1993). "Design of steel triangular plate energy absorbers for seismic-resistant construction." *Earthquake Spectra*, 9(3), 505–528.

Zahrai, S. M., and Bruneau, M. (1998). "Seismic retrofit of steel slab-on-girder bridges using ductile end-diaphragms." *Rep. No. OCEERC 98-20*, Ottawa Carleton Earthquake Engineering Research Centre, Ottawa.